Analyst

Accepted Manuscript

This article can be cited before page numbers have been issued, to do this please use: J. Chen, R. Zhu, J. Huang, M. Zhang, H. Liu, M. Sun, L. Wang and Y. Song, *Analyst*, 2015, DOI: 10.1039/C5AN00200A.

ROYAL SOCIETY OF CHEMISTRY

www.rsc.org/analyst

A Glucose Biosensor based on Glucose Oxidase Immobilized on Three-Dimensional Porous Carbon Electrodes

Jingyi Chen, Rong Zhu, Jia Huang, Man Zhang, Hongyu Liu, Min Sun, Li Wang and Yonghai Song*

Key Laboratory of Functional Small Organic Molecule, Ministry of Education, Key Laboratory of Chemical Biology, Jiangxi Province, College of Chemistry and Chemical Engineering, Jiangxi Normal University, Nanchang, 330022, China.

*Corresponding author: Tel/Fax: +86 791 88120861. E-mail: yhsonggroup@hotmail.com (Y. Song).

Abstract

A novel glucose biosensor was developed by immobilizing glucose oxidase (GOD) on a three-dimensional (3D) porous kenaf stem-derived carbon (3D-KSC) which was firstly proposed as novel supporting materials to load biomolecules for electrochemical biosensing. Here, an integrated 3D-KSC electrode was prepared by using a whole piece of 3D-KSC to load the GOD molecules for glucose biosensing. The morphologies of integrated 3D-KSC and 3D-KSC/GOD electrode were characterized by scanning electron microscopy (SEM) and transmission electron microscopy (TEM). The SEM results revealed 3D honeycomb macroporous structure of integrated 3D-KSC electrode. The TEM results showed some microporosities and defects in the 3D-KSC electrode. The electrochemical behaviors and electrocatalytic performance of integrated 3D-KSC/GOD electrode were evaluated by cyclic voltammetry and electrochemical impedance spectroscopy. The effects of pH and scan rate on the electrochemical response of biosensor have been studied in detail. The glucose biosensor showed a wide linear range from 0.1 mM to 14.0 mM with a high sensitivity of 1.73 μA mM^{-1} and a low detection limit of 50.75 μM. Furthermore, the glucose biosensor exhibited high selectivity, good repeatability and reproducibility, and nice stability.

1. Introduction

The development of glucose detection technique has attracted great interest in recent years due to its expanding practical applications in food and fermentation analysis, textile industry, environmental monitoring, medical diagnosis, etc[1-5]. Many techniques have been used for monitoring glucose level, such as surface plasmon resonance[6], near-infrared spectrum[7], electrochemiluminescene[8], fluorescence[9,10], colorimetry[11], electrochemistry[12-14], etc. Electrochemical biosensors based on biomolecules immobilized on an electrode surface are promising tool owing to their high sensitivity, good selectivity, compatibility for miniaturization, easy operation and low cost. Great efforts have been devoted to immobilization of glucose oxidase (GOD) on an electrode surface, which is one of the main factors that affect the performance of glucose biosensors[12,15,16].

Over the past few years, nanomaterials with high electrical conductivity, large specific surface area and good catalytic activity have been introduced as supporting materials for immobilizing GOD molecules[17-20]. Among various nanomaterials, graphene has shown enormous potential for immobilization of GOD owing to its large specific surface area, two-dimensional honeycomb lattice and excellent electrical conductivities[21,22]. For example, Liu et al. reported a novel highly efficient glucose biosensor by covalently attaching amines of GOD to carboxyl groups of graphene oxide sheets[23]. Shan et al. also constructed a graphene-based electrochemical glucose biosensor with low detection limit[24]. However, graphene nanosheets were apt to aggregate after they were dropped on electrode surface due to strong van der Waals' forces and π– π interactions between individual sheets[20]. Accordingly, the performance of graphene-based electrochemical glucose biosensor could only be improved to some extent. Carbon nanotubes (CNT), showing some good properties similar to graphene, have also been extensively employed for immobilization of GOD[25-28]. Although the

View Article Online
DOI: 10.1039/C5AN00200A

close-packed structures could be suppressed appropriately, it still could not meet the present demand to construct glucose biosensor with high-performance.

Biomass-derived three-dimensional (3D) porous carbon (PC) has attracted special attention because it could be cheaply prepared from a wide variety of low cost precursors[29-36]. As commented in our previous work[36], the 3D kenaf stem-derived (KS) PC (3D-KSC) electrodes showed potential for applications in electrocatalysis, energy storage, electrochemical sensor and capacitor devices because of their large specific surface area, 3D porous structure, low-cost and environmental friendliness. Although the 3D-KSC electrodes have been used as a supporting material to construct a series of 3D-KSC/inorganic nanocomposites for electrochemical sensing platform[36], they have not been explored to load biomolecules for electrochemical biosensing. It is well known that the development of new supporting materials to effectively load a large number of biomolecules on the electrode is very important for electrochemical biosensors.

Herein, a novel electrochemical glucose biosensor was developed by employing low-cost, renewable and environmentally friendly integrated 3D-KSC electrode as a new supporting material to effectively load GOD molecules. As shown in Fig.S1 (ESI$^+$), a whole piece of 3D-KSC was used to prepare an integrated 3D-KSC electrode and accordingly the complete 3D macroporous structure was kept, which provided a large specific surface area to immobilize a large number of GOD molecules effectively and improved mass transfer greatly. Some microporosities and defects in the 3D-KSC electrodes enhanced the immobilization of GOD molecules greatly. Therefore, the 3D-KSC electrodes could be used to immobilize GOD molecules better and the resulted biosensor showed superior electrochemical performance with good stability and reproducibility. It is first time that the 3D-KSC electrodes were used to immobilize biomolecules (eg. GOD molecules) for electrochemical biosensing.

View Article Online
DOI: 10.1039/C5AN00200A

2 Experimental

2.1 Reagents and materials

Kenaf (hibiscus cannabinus) stems (KS) were obtained from a local farm (Futian, China) directly. Glucose oxidase (GOD, EC 1.1.3.4, 140 U mg^{-1}) and nafion (5 wt.%) were obtained from Sigma. Graphite powder (99.95%, 325 mesh) was purchased from Aladdin Ltd. (Shanghai, China). Potassium ferricyanide ($K_3Fe(CN)_6$), potassium chloride (KCl), ascorbic acid (AA), uric acid (UA), mannose, fructose, lactose, glucose, etc, were obtained from Beijing Chemical Reagent Factory (Beijing, China). All reagents were of analytical grade and used as received. Phosphate buffer solutions (PBS, 0.2 M, pH 7.0) were prepared with 0.2 M NaH_2PO_4 and 0.2 M Na_2HPO_4. GOD solution (65 μM) was prepared in 0.2 M PBS (pH 7.0). All solutions were prepared with ultra-pure water purified by a Millipore-Q System (18.2 MΩ cm).

2.2 Preparation of integrated 3D-KSC/GOD electrodes

The 3D-KSC was prepared by carbonization of dried KS at a high-temperature furnace according to our previous work[36]. The carbonization process was conducted in a tubular quartz reactor under N_2 atmosphere with a heating rate of 5 °C min^{-1} and annealing for 2 h at 900 °C. The 3D-KSC was cut into cylinder with the outside diameter almost equal to the inside diameter of treated pipette tip and accordingly the cylindrical 3D-KSC could be immobilized in treated pipette tip firmly. The processed 3D-KSC was washed with ethanol and ultra-pure water alternately, dried naturally, and inserted into the treated pipette tip leaving about 0.2 mm long part outside. Then 1.0 g graphite powder and 0.25 g liquid paraffin were mixed and homogenized carefully in an agate mortar for 20 min. After that, the homogenized mixture was packed into the upper part of pipette tip to contact the end of 3D-KSC. Here, about 0.2-0.3 mm long bottom of the pipette tip have no homogenized mixture and accordingly the pasty mixture did not flow out. And then, a copper wire was inserted into the pipette tip to electrically connect with the end of 3D-KSC via the graphite powder. After the homogenized mixture paste was naturally dried at room temperature, the copper wire was further immobilized by using parafilm or epikote as shown in Fig. S1 (ESI^+). Finally, a thin layer of

transparent nail polish was coated on the gap between the treated pipette tip and the 3D-KSC in order to avoid the solution into the treated pipette tip. The schematic structure of the 3D-KSC electrode was illustrated in detail in Fig. S1 (ESI^+). The 3D-KSC electrode was immersed into 65 μM GOD solution at 4 ºC for 12 h. Finally, the modified electrode was rinsed by ultra-pure water to remove weakly bound molecules and stored at 4 ºC for further use. The resulted electrode was referred as 3D-KSC/GOD electrode. The preparation procedure was also illustrated in Fig. S1 (ESI^+).

2.3 Apparatus

Cyclic voltammograms (CVs) and electrochemical impedance spectroscopy (EIS) were carried out with a CHI750D electrochemical workstation (CHI, China). A three-electrode configuration was used with a platinum wire as the auxiliary electrode, a saturated calomel electrode (SCE) as the reference electrode, and a 3D-KSC/GOD electrode as the working electrode. The effective surface areas (A_{eff}) of various 3D-KSC were estimated before use based on the CVs in 0.1 M KCl solution containing 5.0 mM $Fe(CN)_6^{3-/4-}$ at 50 mV s^{-1} according to Randles-Sevcik equation as shown in Fig. S2 (ESI^+). The currents have been normalized based on the A_{eff}. Other CVs was carried out in 10.0 mL of 0.2 M PBS (pH 7.0) at room temperature. EIS was characterized at open circuit potential in the frequency range from 0.01 Hz to 10^5 Hz with the amplitude 5 mV. The scanning electron microscopy (SEM) analysis was taken using a XL30 ESEM-FEG SEM at an accelerating voltage of 20 kV equipped with a Phoenix energy dispersive X-ray analyzer (EDXA). Transmission electron microscopy (TEM) images were taken on JEOL JEM-2100 microscopes operated at an acceleration voltage of 200 KV.

3 Results and discussion

3.1 Characterization of 3D-KSC/GOD electrodes

The SEM was firstly employed to investigate the morphology of 3D-KSC and 3D-KSC/GOD electrode. As shown in Fig. 1A-C, many macropores appeared in the 3D-KSC electrode, revealing

View Article Online
DOI: 10.1039/C5AN00200A

the hollow structure inside. Their diameters were estimated to be about 10 μm. The TEM image clearly revealed many black and white spots on the 3D-KSC (Fig. S3, ESI$^+$), which indicated microporous structures and some defects in the graphite nanosheets. Magnified SEM images (Fig. 1B and C) showed that the inner wall of pores was smooth. When GOD molecules were assembled on the 3D-KSC electrode, the inner wall of pores in the 3D-KSC/GOD electrode became rough and uneven with an opaque layer of fuzzy-like substance which might result from the adsorption of GOD molecules on inner wall of pores (Fig. 1E and F). Moreover, the structure of GOD molecules might be destroyed when electron beam pierced the protein and accordingly the pore surfaces of 3D-KSC/GOD electrode became fuzzy. The results clearly demonstrated the successful immobilization of GOD molecules on the 3D-KSC electrode.

"Here in Fig. 1"

3.2 Electrochemical behaviors of 3D-KSC/GOD electrodes

The EIS has been a popular tool to monitor the electrode assembly process due to its immediate and sensitive response to the electrode surface changes[37]. Fig. 2 showed the EIS of 3D-KSC/GOD electrode (curve a) and 3D-KSC electrode (curve b) in 5 mM $Fe(CN)_6^{3-/4-}$ containing 0.1 KCl as supporting electrolyte. The inset showed a Randles equivalence circuit model which was chosen to fit the impedance data[38]. In the Randles circuit, the resistance to charge transfer (R_{ct}) and the diffusion impedance (W) were both assumed in parallel to the interfacial capacity (C_{dl}). The parallel structure of R_{ct} and C_{dl} gave rise to a semicircle in the complex plane plot of Z_{im} against Z_{re}. The R_{ct} of 3D-KSC electrode (25 Ω, curve b) was extremely small. After the GOD was coated on the 3D-KSC electrode surface, an obvious increase of R_{ct} (75 Ω, curve a) was observed. It might be ascribed not only to hindrance of GOD molecule layer to $Fe(CN)_6^{3-/4-}$ but also to electrostatic repulsion between $Fe(CN)_6^{3-/4-}$ and negatively charged GOD molecules[39]. Therefore, the increase of R_{ct} also indicated that the successful immobilization of GOD molecules on the surface of

3D-KSC electrode.

"Here in Fig. 2"

Fig. 3A showed the CVs of 3D-KSC/GOD electrode in 0.2 M N_2-saturated PBS with pH from 6.0 to 8.0 at a scan rate of 100 mV s^{-1}. The formal potential ($E^0 = (E_{pa} + E_{pc})/2$) displayed a linear relativity to pH with slope of -58.64 mV/pH ($R = -0.999$) (inset of Fig. 3A). This value was very close to the theoretical value of −58.6 mV/pH for the two-electron and two-proton transportation process of FAD/$FADH_2$ redox couples in the GOD[40]. The effect of the potential scan rate on the electrochemical performance of 3D-KSC/GOD electrode was shown in Fig. 3B. The redox peak current increased linearly as the potential scan rate increased from 50 to 1000 mV s^{-1} (inset of Fig. 3B), indicating a quasi-reversible surface-controlled electrochemical process[41]. The surface coverage (Γ, in mol cm^{-2}) of GOD on the 3D-KSC electrode could be determined based on Faraday's law:[41]

$$I_P = \frac{nFQv}{4RT} = \frac{n^2F^2A\Gamma^*v}{4RT} \quad (1)$$

This equation could be transferred as the following expression:

$$\Gamma^* = \frac{Q}{nFA} \quad (2)$$

where Q is the charge consumed in the CVs, n is the electron transfer number (n=2 for direct electron transfer of GOD which has been proven by above result), F is Faraday constant (F = 96493 C mol^{-1} [41]) and A_{eff} is the effective surface areas of the electrode. The Γ value of 3D-KSC/GOD electrode was calculated to be 3.99×10^{-10} mol cm^{-2} which was much higher than the theoretical molecular monolayer surface coverage (1.4×10^{-12} mol cm^{-2}). The large Γ might be ascribed to the 3D porous structure of integrated 3D-KSC electrode which provided a large specific surface area to effectively immobilize a large number of GOD molecules. Moreover, some microporosities and

View Article Online
DOI: 10.1039/C5AN00200A

defects in the integrated 3D-KSC electrode might also enhance the immobilization of GOD molecules.

At scan rate of 100 mV s^{-1}, the ΔE_p=33 mV and $n\Delta E_p$=66 mV < 200 mV, the electron transfer coefficient (α_s) was determined to be 0.5. The electron-transfer rate constant (k_s) could be estimated based on Laviron theory[42]:

$$k_s = mnF\upsilon/RT \quad (3)$$

where n is the electron transfer number (n=2), F is Faraday constant (F = 96493 C mol^{-1}), υ is the scan rate, R is the gas constant (R = 8.314 J mol^{-1} K^{-1}), T is the temperature in Kelvin (T = 298 K) and m is a constant which relates to ΔE_p. The k_s was calculated to be 3.45 s^{-1} for the 3D-KSC/GOD electrode, larger than that of previous reported gelatin-multi-walled carbon nanotube /GOD/glutaraldehyde/GCE of 1.08 s^{-1} [25] and GOD/PDDA/multi-walled carbon nanotube (MWCNT)-AuNPs/GCE of 1.01 s^{-1} [43]. The results indicated that the 3D-KSC electrode did promote the electron transfer of GOD molecules. The fast electron transfer might be attributed to the 3D porous structure of 3D-KSC electrode which improved the diffusion of electrolyte between GOD and electrode surface to help for the electron transfer. The good electrical conductivity of 3D-KSC electrode[36] and uniform distribution of GOD molecules on the 3D-KSC electrode further enhanced the electron transfer.

"Here in Fig. 3"

3.3 Electrocatalytic properties of 3D-KSC /GOD electrodes

As shown by the pink curve in Fig. 4A, the CVs of 3D-KSC/GOD electrode exhibited an obvious cathodic peak and a disappeared anodic peak in the presence of O_2, indicating a typical electrocatalytic reduction of O_2[44]. The cathodic current decreased gradually with the increase of glucose concentration, indicating the consumption of O_2. Thus, the glucose could be catalytically oxidized into gluconolactone by GOD on the 3D-KSC/GOD electrode and the generated

GOD($FADH_2$) could be oxidized into GOD(FAD) by O_2. The possible mechanism could be shown by following equations[45,46].

$$\text{Glucose} + \text{GOD (FAD)} \longrightarrow \text{Gluconolactone} + \text{GOD } (FADH_2) \quad (4)$$

$$\text{GOD } (FADH_2) + O_2 \longrightarrow \text{GOD (FAD)} + H_2O_2 \quad (5)$$

In total:

$$\text{Glucose} + O_2 \xrightarrow{\text{GOD}} \text{gluconolactone} + H_2O_2 \quad (6)$$

The 3D-KSC/GOD electrode could be used to detect glucose based on the changes of O_2 reduction peak current[47]. Fig. 4A and (Fig. S4, ESI^+) showed the CVs of 3D-KSC/GOD electrode in O_2-saturated 0.2 M PBS (pH 7.0) with various concentrations of glucose at a scan rate of 50 mV s^{-1}. As shown in Fig. 4B, the cathodic peak current decreased linearly with the increase of glucose concentration from 0.1 to 14.0 mM with a sensitivity of 1.73 μA mM^{-1}. The detection limit was estimated to be about 50.75 μM based on the criterion of signal-to-noise ratio of 3. A large number of GOD molecules immobilized on the porous structure of 3D-KSC electrode might result in the wide linear range and the low detection limit.

To exhibit the advantages of proposed biosensor, the analytical performances of developed biosensor were compared with other glucose sensors in Table 1. Results illustrated that the designed biosensor exhibited a wide linear range and a high sensitivity toward glucose detection. As discussed above, some defects and microporosities in the 3D-KSC electrode resulted in a good adsorption for GOD molecules. The 3D porous structure of 3D-KSC might improve the mass transfer and provide a large specific surface area to effectively load a large number of GOD molecules. The good electrical conductivity of 3D-KSC electrode[36] and uniform distribution of GOD molecules further enhanced the electron transfer. As a consequence, the developed biosensor has a good performance. Furthermore, the synthesis of other carbon materials was always complex. and the 3D-KSC was a kind of natural and simple-fabricated material. As could be seen, the

View Article Online
DOI: 10.1039/C5AN00200A

comparison of analytical performance of our proposed glucose biosensors with selected ones that have been proposed by others in earlier publications in Table 1 perhaps don't have a very clearly significant advancement. However, it is possible that further treatment by N-doping or fabricating a lot of porosities or defects in the 3D-KSC electrode should improve the performance of our developed biosensor.

"Here in Fig. 4"

"Here in Table 1"

3.4 Repeatability, reproducibility and stability of the biosensor

Electrochemical experiments have been repeated for 6 times to ensure the reliability of data. Here, the KSC-GOD electrodes were made not only by using one batch of pyrolyzed KS but also by using different batches of pyrolyzed KS. The electrochemical results indicated that these 3D-KSC/GOD electrodes had no obvious difference (Fig. S5, ESI$^+$). And the relative standard deviation (RSD) was about 4.68 %. The repeatability of biosensor was investigated by successively detecting 5.0 mM glucose for 6 times, and the RSD was about 3.68 %, indicating a good repeatability. The current responses were checked daily up to 10 days, and the current response was still retained 97.4 % value of the initial response. The results indicated that the 3D-KSC/GOD electrode showed good repeatability, reproducibility and stability.

3.5 Interference and glucose detection in human blood serum

Some possibly coexisting materials such as some carbohydrates, AA and UA were used to test the selectivity of the glucose biosensor. The 3D-KSC/GOD electrode was first kept in a stirred 0.2 M O_2-saturated PBS (pH 7.0) at scan rate of 100 mV s^{-1} and then a 2.0 mM glucose solution was added. After that, 6.0 mM UA, 6.0 mM AA, 6.0 mM fructose, 6.0 sucrose and 6.0 mM mannose were added sequentially. The results indicated that the possibly coexisted materials have no obvious interference for the detection of glucose as shown in Fig 5 and Fig. S6 (ESI$^+$). Hence, a highly

selective response to glucose was obtained without the use of a perm-selective membrane or enzymatic preoxidation.

In order to evaluate the practical application of developed biosensor in clinical analysis, the 3D-KSC/GOD electrode was utilized to detect glucose in human serum samples without any pretreatment except a dilution step (2-fold with PBS). The concentration of glucose in a serum sample was determined to be 2.76 mM which was close to the standard value of 2.69 mM determined by colorimetric enzymatic method. To evaluate the accuracy of developed glucose biosensor, different amounts of glucose were added into human serum samples for recovery tests. The test results from four repeated experiments were listed in Table S1 and Fig. S7 (ESI^+), which showed acceptable recoveries between 97.7% and 109% and the RSD lower than 4.47%. The results indicated that the method we developed was reliable and applicable in real human sample analysis.

"Here in Fig. 5"

4. Conclusion

In summary, a promising glucose biosensor based on GOD molecules immobilized on the 3D-KSC electrode was successfully achieved. The results proved that the integrated 3D-KSC electrode could be used to effectively load a large number of biomolecules for electrochemical biosensing. The 3D porous structure obviously improved the mass transfer. The excellent conductivity was favorable for electron transfer between biomolecules and electrode surface. Some defects and microporosities formed in the 3D-KSC electrode resulted in a good adsorption of GOD molecules. The CVs results showed a pair of well-defined redox peaks corresponding to the electron transfer of GOD, which indicated that the direct electron transfer between GOD and the 3D-KSC electrode could be achieved. With wide linear range, high sensitivity and good selectivity, the new designed biosensor might be used for the detection of glucose concentrations in practical

samples. Moreover, it is possible to fabricate other analogous enzyme electrode based on the integrated 3D-KSC electrode.

View Article Online
DOI: 10.1039/C5AN00200A

Acknowledgments

This work was financially supported by National Natural Science Foundation of China (21165010, 21465014 and 21465015), Natural Science Foundation of Jiangxi Province (20142BAB203101), The Ministry of Education by the Specialized Research Fund for the Doctoral Program of Higher Education (20133604110002) and the Ground Plan of Science and Technology Projects of Jiangxi Educational Committee (KJLD14023), the Open Project Program of Key Laboratory of Functional Small Organic Molecule, Ministry of Education, Jiangxi Normal University (No. KLFS-KF-201410; KLFS-KF-201416), and Innovation Foundation for Graduate Student of Jiangxi Province and Jiangxi Normal University (YC2014-S159).

Reference

1. J. Wang, *Chem. Rev.*, 2008, **108**, 814-825.

2. C. Guo, H. Huo, X. Han, C. Xu and H. Li, *Anal. Chem.*, 2014, **86**, 876–883.

3. W. Lu, X. Qin, A.M. Asiri, A.O. Al-Youbi and X. Sun, *Analyst*, 2013,**138**, 417-420..

4. L. Wang, X. Lu, C. Wen, Y. Xie, L. Miao, S. Chen, H. Li, P. Li and Y. Song, *J. Mater. Chem. A*, 2015, **3**, 608-616.

5. Y. Song, H. Liu, H. Tan, F. Xu, J. Jia, L. Zhang, Z. Li and Li Wang, *Anal. Chem.,* 2014, **86**, 1980-1987.

6. H. He, X. Xu, H. Wu, Y. Zhai and Y. Jin, *Anal. Chem.,* 2013, **85**, 4546-4553.

7. M. Mesch, C. Zhang, P. V. Braun and H. Giessen, *ACS Photonics*, 2015, **2**, 475–480.

8. J. Kremeskotter, R. Wilson, D. Schiffrin, B. J. Luff and J. S. Wilkinson, *Meas. Sci. Technol.*, 1995, **6**, 1325.

9. S. Joel, K. B. Turner and S. Daunert, *ACS Chem. Biol.*, 2014, 9, 1595–1602.

10. M. Lan, J. Zhang, Y.-S. Chui, H. Wang, Q. Yang, X. Zhu, H. Wei, W. Liu, J. Ge, P. Wang, X. Chen, C.-S. Lee and W. Zhang, *J. Mater. Chem. B*, 2015, **3**, 127-134.

11. Y. Xia, J. Ye, K. Tan, J. Wang and G. Yang, *Anal. Chem.*, 2013, **85**, 6241–6247.

12. W. Ma, Q. Jiang, P. Yu, L. Yang and L. Mao, *Anal. Chem.*, 2013, **85**, 7550–7557.

13. X. Niu, M. Lan, H. Zhao and C. Chen, *Anal. Chem.*, 2013, **85**, 3561–3569.

14. X. Gao, N. Wang, S. Jia and Y. Shao, *Anal. Chem.*, 2013, **85**, 5040-5046.

15. Y. Song, H. Liu, Y. Wang and L. Wang, *Electrochim. Acta*, 2013, **93**, 17-24.

16. P. Yang, L. Wang, Q. Wu, Z. Chen and X. Lin, *Sens. Actuators, B*, 2014, **194**, 71-78.

17. D. Xiang, L. Yin, J. Ma, E. Guo, Q. Li, Z. Li and K. Liu, *Analyst*, 2015, **140**, 644-653.

18. Y. Song, J. Chen, H. Liu, Y. Song, F. Xu, H. Tan and L. Wang, *Electrochim. Acta*, 2015, **158**,

56-63.

19. S. Palanisamy, C. Karuppiah and S.-M. Chen, *Colloids Surf., B*, 2014, **114**, 164-169.

20. Y. Xu, H. Bai, G. Lu, C. Li and G. Shi, *J. Am. Chem. Soc.*, 2008, **130**, 5856-5857.

21. Q. Xu, S.-X. Gu, L. Jin, Y.-E. Zhou, Z. Yang, W. Wang and X. Hu, *Sens. Actuators, B*, 2014, **190**, 562-569.

22. D. Li, M. B. Mueller, S. Gilje, R. B. Kaner and G. G. Wallace, *Nat. Nanotechnol.*, 2008, **3**, 101-105.

23. Y. Liu, D. Yu, C. Zeng, Z. Miao and L. Dai, *Langmuir*, 2010, **26**, 6158-6160.

24. C. Shan, H. Yang, D. Han, Q. Zhang, A. Ivaska and L. Niu, *Langmuir*, 2009, **25**, 12030-12033.

25. H. Wang, Q. Lang, L. Li, B. Liang, X. Tang , L. Kong, M. Mascini and A. Liu, *Anal. Chem.*, 2013, **85**, 6107–6112.

26. M. Zhao, Y. Gao, J. Sun and F. Gao, *Anal. Chem.*, 2015, **87**, 2615-2622.

27. X. Lu, H. Cheng, P. Huang, L. Yang, P. Yu and L. Mao, *Anal. Chem.*, 2013, **85**, 4007–4013.

28. J. M. Goran, S. M. Mantilla and K. J. Stevenson, *Anal. Chem.*, 2013, **85**, 1571–1581.

29. M. Sevilla, A. Fuertes and R. Mokaya, *Energy Environ. Sci.*, 2011, **4**, 1400-1410.

30. Z. Wang, P. Dornath, C.-C. Chang, H. Chen and W. Fan, *Micropor. Mesopor. Mat.,* 2013, **181** 8-16.

31. Y. Wang, S. Tao and Y. An, *Micropor. Mesopor. Mat.*, 2012, **163**, 249-258.

32. L. Wang, Y. Zheng, S. Chen, Y. Ye, F. Xu, H. Tan, Z. Li, H. Hou and Y. Song, *Electrochim. Acta*, 2014, **135**, 380-387.

33. A. Stein, Z. Wang and M. A. Fierke, *Adv. Mater.*, 2009, **21**, 265-293.

34. M. Sevilla and A. B. Fuertes, *Energy Environ. Sci.*, 2011, **4**, 1765-1771.

35. S. Chen, Q. Liu, G. He, Y. Zhou, M. Hanif, X. Peng, S. Wang and H. Hou, *J. Mater. Chem.*,

2012, **22**, 18609-18613.

36. L. Wang, Q. Zhang, S. Chen, F. Xu, S. Chen, J. Jia, H. Tan, H. Hou and Y. Song, *Anal. Chem.*, 2014, **86**, 1414-1421.

37. W. R. Yang, J. J. Gooding and D. B. Hibbert, *J. Electroanal. Chem.*, 2001, **516**, 10-16.

38. H. O. Finklea, D. A. Snider, J. Fedyk, E. Sabatani, Y. Gafni and I. Rubinstein, *Langmuir*, 1993, **9**, 3660-3667.

39. X. Kang, J. Wang, H. Wu, I. A. Aksay, J. Liu and Y. Lin, *Biosen. Bioelectron.*, 2009, **25**, 901-905.

40. C. Deng, J. Chen, Z. Nie and S. Si, *Biosen. Bioelectron.*, 2010, **26**, 213-219.

41. R. Freeman, B. Willner and I. Willner, *J. Phys. Chem. Lett.*, 2011, **2**, 2667-2677.

42. E. Laviron, *J. Electroanal. Chem.*, 1979, **101**, 19-28.

43. Y. L. Yao and K. K. Shiu, *Electroanalysis*, 2008, **20**, 1542-1548.

44. Q. Zeng, J.-S. Cheng, X.-F. Liu, H.-T. Bai and J.-H. Jiang, *Biosen. Bioelectron.*, 2011, **26**, 3456-3463.

45. M. Wooten, S. Karra, M. Zhang and W. Gorski, *Anal. Chem.*, 2014, **86**, 752-757.

46. F. Qu, Y. Zhang, A. Rasooly and M. Yang, *Anal. Chem.*, 2014, **86**, 973-976.

47. L.-M. Liu, J. Wen, L. Liu, D. He, R.-Y Kuang and T. Shi, *Anal. Biochem.*, 2014, **445**, 24-29.

48. C. Yang, C. Xu and X. Wang, *Langmuir*, 2012, **28**, 4580-4585.

49. Y. Wang, L. Liu, M. Li, S. Xu and F. Gao, *Biosens. Bioelectron.*, 2011, **30**, 107-111.

50. Y. Wang, H.X. Li and J.L. Kong, *Sens. Actuators, B*, 2014, **193**, 708-714.

51. C. Shan, H. Yang, D. Han, Q. Zhang, A. Ivaska and L. Niu, *Biosens. Bioelectron.*, 2010, **25**, 1070-1074.

52. M. D. Rubianes and G. A. Rivas, *Electrochem. Commun.,* 2003, **5**, 689-694.

53. J. Wang, L. Wang, J. Di and Y. Tu, *Sens. Actuators, B*, 2008, **135**, 283-288.

View Article Online
DOI: 10.1039/C5AN00200A

54. H. Wang, X. Wang, X. Zhang, X. Qin, Z. Zhao, Z. Miao, N. Huang, Q. Chen, *Biosens. Bioelectron.*, 2009, **25**, 142-146.

55. A. Salimi, R.G. Compton and R. Hallaj, *Anal. Biochem.*, 2004, **333**, 49-56.

View Article Online
DOI: 10.1039/C5AN00200A

Table 1 Comparison of analytical performance of some GOD-based glucose biosensors.

Glucose biosensors	Detecting limit (μM)	Linear range (mM)	Reference
GOD/MWCNT-chitosan	20	1.0-10.0	[48]
GOD/graphene-CdS	700	2.0-16.0	[49]
Nafion-mesocellular graphene foam-GOD/GCE	250	1.0-12	[50]
GOD-graphene-AuNPs-chitosan	180	2-10	[51]
GOD– carbon nanotubes paste electrodes	600	0-25	[52]
GOD/cysteame/AuNPs/ITO	15	0.04-4.80	[53]
GOD/BSA/ AuNPs -Pb NWs/Pt	2	0.05-2.2	[54]
GOD-Sol-Gel-CNTs electrode	50	0.2-20	[55]
Graphene/AuNPs/chitosan/Au electrode	180	2-14	[51]
GOD/KSC electrode	50.75	0.1 -14.0	In this work

View Article Online
DOI: 10.1039/C5AN00200A

Figure captions

Fig. 1. SEM images of (A-C) 3D-KSC and (D-F) 3D-KSC/GOD electrode.

Fig. 2. EIS of 3D-KSC/GOD electrode (curve a) and 3D-KSC electrode (curve b) in 5.0 mM $Fe(CN)_6^{3-/4-}$ containing 0.1 KCl. Inset is the equivalent circuit.

Fig. 3. (A) CVs of 3D-KSC/GOD modified electrode in 0.2 N_2-saturated PBS with pH from 6.0 to 8.0 at a scan rate of 50 mV s^{-1} (from left to right: pH 8.0, 7.5, 7.0, 6.5 and 6.0). Inset: plot of pH versus $E^{\theta'}$. (B) CVs of 3D-KSC/GOD electrode in 0.1 M N_2-saturated PBS (pH 7.0) at different scan rates (from inner to outer: 50, 100, 200, 300, 400, 500, 600, 700, 800, 900 and 1000 mV s^{-1}) Inset: linear dependence of I_{pa} and I_{pc} on scan rates.

Fig. 4. (A) CVs of 3D-KSC/GOD electrode and (B) calibration curve in 0.2 M O_2-saturated PBS (pH 7.0) at scan rate of 50 mV s^{-1} in the presence of glucose with various concentrations. The potential chosen reading done for calibration curve construction was -0.5 V.

Fig. 5. Comparison of CVs response of 3D-KSC/GOD in 0.2 M O_2-saturated PBS in the presence of glucose and other interfering substances.

View Article Online
DOI: 10.1039/C5AN00200A

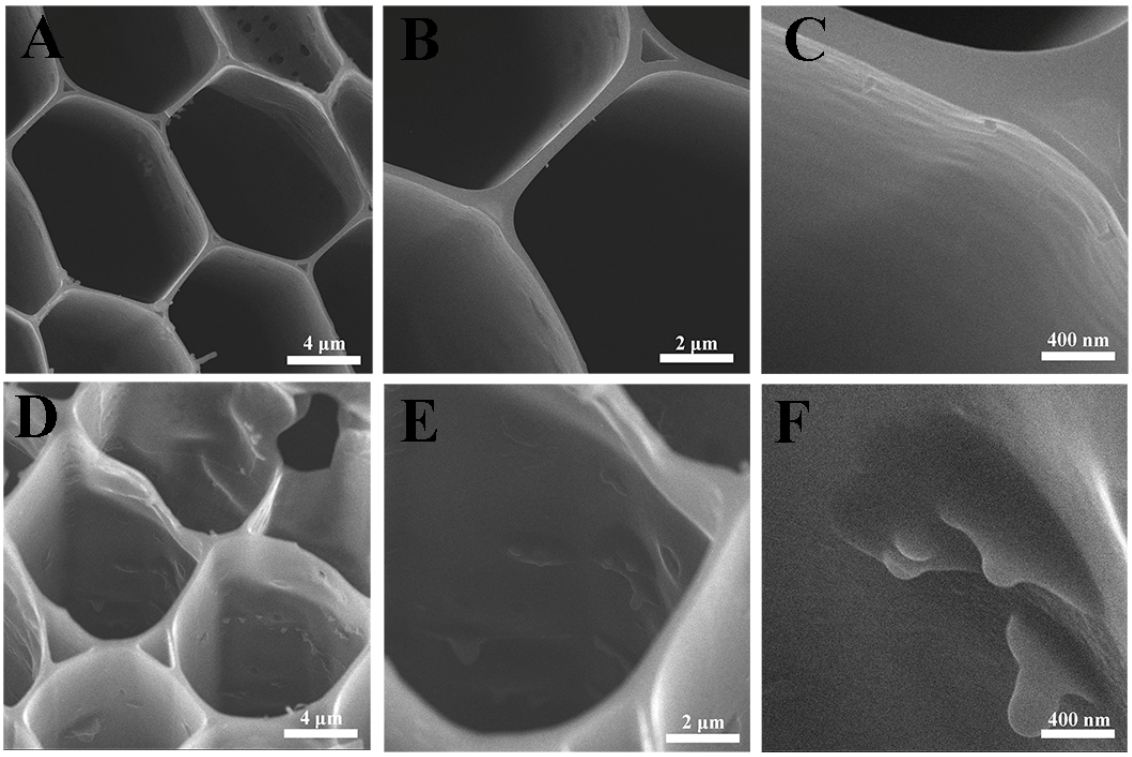

Fig. 1

View Article Online
DOI: 10.1039/C5AN00200A

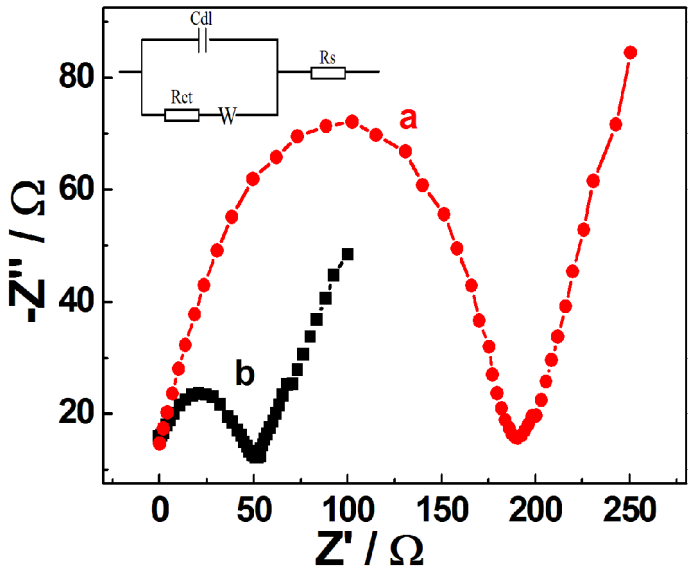

Fig. 2

View Article Online
DOI: 10.1039/C5AN00200A

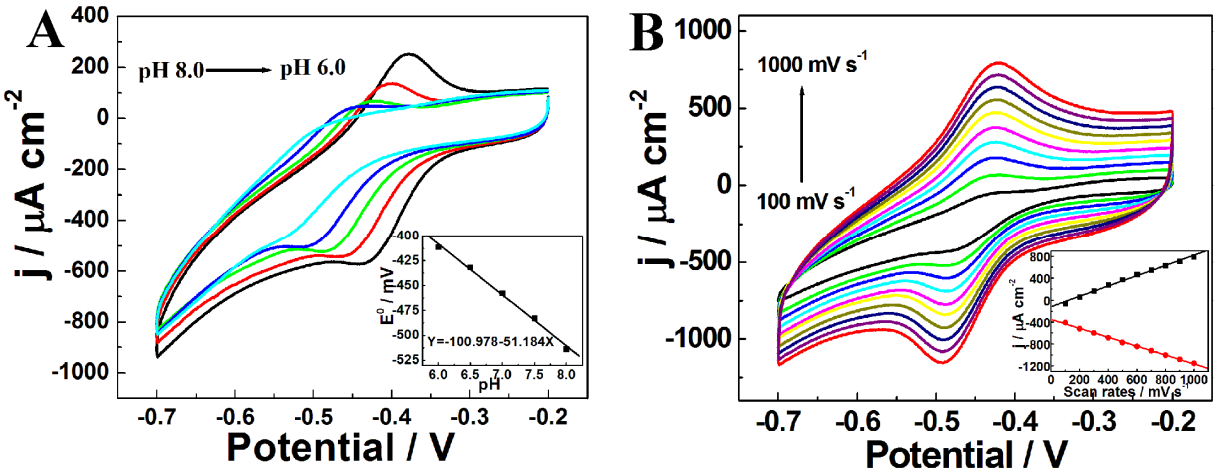

Fig. 3

View Article Online
DOI: 10.1039/C5AN00200A

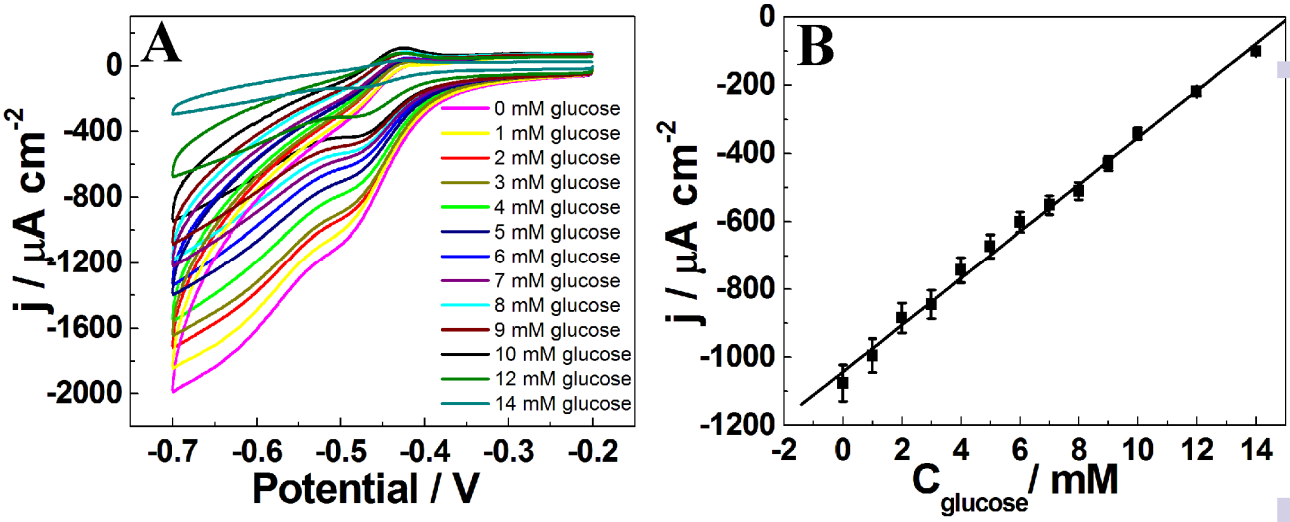

Fig. 4

View Article Online
DOI: 10.1039/C5AN00200A

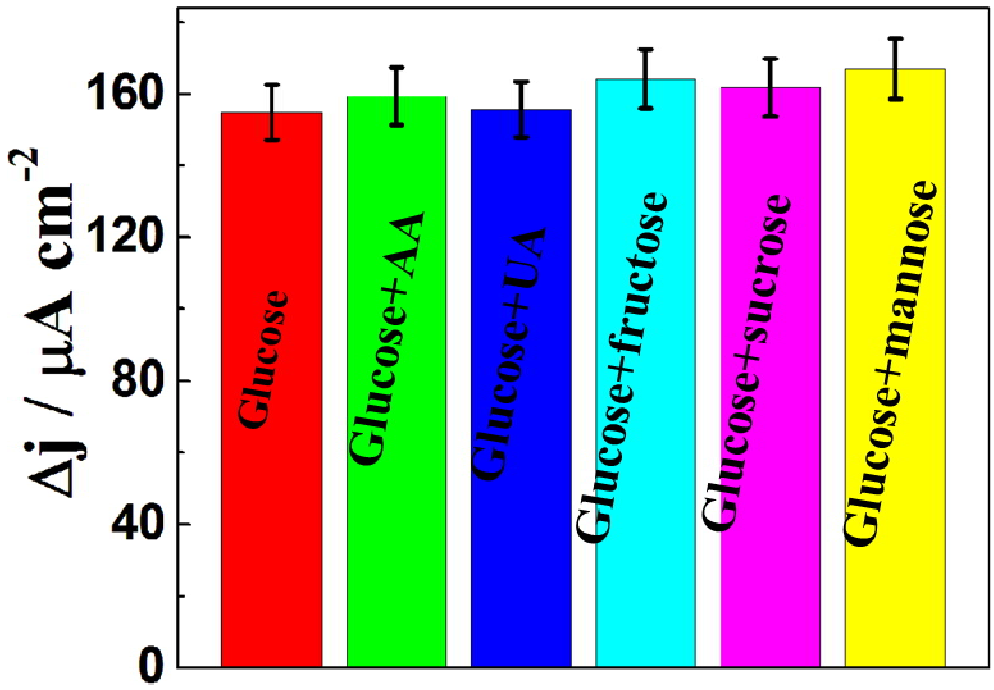

Fig. 5